"LA-UR -91-847

LA-UR--91-847

DE91 009947

TITLE: An Expanding Grid Photochemical Model for Visibility Applications

AUTHOR(S): M. D. Williams

SUBMITTED TO: 84th Annual Meeting of the Air & Waste Management Association, Vancouver, B.C., June 16-21, 1991.

DISCLAIMER

Los Alamos National Laboratory
Los Alamos, New Mexico 87545

91-51.1

AN EXPANDING GRID PHOTOCHEMICAL MODEL FOR VISIBILITY APPLICATIONS

Michael D. Williams
Los Alamos National Laboratory
Group A-4
Mail Stop B299
Los Alamos, NM 87545

Gerald Streit
Los Alamos National Laboratory
Group A-4
Mail Stop B299
Los Alamos, NM 87545

March 1, 1991

INTRODUCTION

The photochemistry of plumes has been important for several years. Of primary concern is the formation of secondary pollutants in plumes. Among the species of interest are sulfates, nitrates, and oxidants. Sulfates and nitrates can contribute to acid deposition and sulfates can also produce visibility impairment. Oxidants, such as ozone and peroxyacetylnitrate, are linked to health and vegetation effects.

Davis[1] reported ozone formation in an eastern power plant plume several years ago and suggested a reaction pathway which involved free radical and sulfur chemistry. He reported depletion of ozone in the early part of the plume travel followed by formation of an ozone bulge on the sides of the plume. At large distances downwind he found an ozone increase as the plume was traversed. However, his proposed mechanism has not been supported by other studies and power plant plumes in the southwest have generally not exhibited ozone increases. One plume[2] in the southwest did seem to have an ozone bulge at large downwind distances.

Photochemical models for visibility applications normally suffer from several limitations which impair their application to point source plumes. Lagrangian type models suffer from an inability to handle wind shear and reversing winds while Eulerian based systems smear the plume unrealistically during the early part of its travel. To avoid these problems a new model has been developed and compared to measurements near a southwestern power plant. The new system is quasi- Lagrangian in that the grid at any point in time covers the volume occupied by contaminants at that time. Consequently, the modeled volume is small during the early portion of the plume and expands with time. However, unlike Lagrangian models, the modeled volume is described by cells among which contaminants are both advected and diffused and to which new plume material can be added.

The model is driven by winds, temperatures, and turbulences provided by a three-dimensional, prognostic, higher order turbulence, atmospheric circulation model (HOTMAC). Consequently, it can describe plume travel and dispersion in complex terrain and over a diurnal cycle.

The modeling system is designed to deal with the complexities which occur when portions of the plume arrive at the same point with different histories. For example, material near the surface may have a much slower velocity than material aloft, but during the daytime,

mixing can bring the materials together. An additional complexity, which the model treats, is different behavior found within a plume. In the interior of the plume, high concentrations of nitric oxide may minimize reactions which form aerosols, while on the edges of the plume the reaction rates may be much greater.

The chemistry description in the model is based upon the carbon-bond IV mechanism[3] with additional reactions for methane, sulfur chemistry, aerosol formation, and aerosol growth. The model has been applied to the Grand Canyon region where wind-shears and diurnal changes in direction produce very complex pollutant trajectories.

THE METEOROLOGICAL MODELING SYSTEM

Model Formulation

HOTMAC is a three-dimensional time-dependent model developed by T. Yamada[4]. It uses the hydrostatic approximation and a terrain following coordinate system in which the vertical coordinate z^*, is given by:

$$z^* = H\frac{z - z_g}{H - z_g} \tag{1}$$

where z_g is the height of the ground and H is the height of the top of model domain. H is equal to H minus the height of the highest terrain in the domain.

HOTMAC solves conservation relations for the horizontal wind components, potential temperature, moisture, turbulent kinetic energy, and the turbulence length scale. HOTMAC describes advection, coriolis effects, turbulent transfer of heat, momentum, and moisture. It also describes solar and terrestrial radiation effects, turbulent history effects, and drag and radiation effects of forest canopies.

Equation 2 represents the conservation equation for the east-west component of momentum. The total rate of change of the u component of the wind is equal to the sum of a coriolis term, a buoyancy term, two horizontal eddy transport terms and a vertical momentum transport term.

$$\frac{DU}{Dt} = f(V - V_g) + g\frac{H - z^*}{H}\left(1 - \frac{\langle\Theta_v\rangle}{\Theta_v}\right)\frac{\partial z_g}{\partial x} \tag{2}$$

$$+\frac{\partial}{\partial x}\left(K_x\frac{\partial U}{\partial x}\right)+\frac{\partial}{\partial y}\left(K_{xy}\frac{\partial U}{\partial y}\right)+\frac{\overline{H}}{H-z_g}\frac{\partial}{\partial z^*}(-\overline{uw}).$$

V_g is the north-south component of the geostrophic wind. $\langle\theta_v\rangle$ is the horizontal average of the virtual potential temperature. Equation 3 is a similar expression for the north-south components of momentum.

$$\frac{DV}{Dt}=-f(U-U_g)+g\frac{\overline{H}-z^*}{\overline{H}}\left(1-\frac{\langle\Theta_v\rangle}{\Theta_v}\right)\frac{\partial z_g}{\partial y} \tag{3}$$
$$+\frac{\partial}{\partial x}\left(K_{xy}\frac{\partial V}{\partial x}\right)+\frac{\partial}{\partial y}\left(K_y\frac{\partial V}{\partial y}\right)+\frac{\overline{H}}{H-z_g}\frac{\partial}{\partial z^*}(-\overline{vw}).$$

Equation 4 is derived from the hydrostatic approximation and it describes the vertical velocity W^*, in the z^* coordinate system.

$$\frac{\partial U}{\partial x}+\frac{\partial V}{\partial y}+\frac{\partial W^*}{\partial z^*}-\frac{1}{H-z_g}\left(U\frac{\partial z_g}{\partial x}+V\frac{\partial z_g}{\partial y}\right)=0. \tag{4}$$

Equation 5 is the energy conservation Equation which describes the total rate of change of the potential temperature.

$$\frac{D\Theta}{Dt}=\frac{\partial}{\partial x}\left[K_x\frac{\partial\Theta}{\partial x}\right]+\frac{\partial}{\partial y}\left[K_y\frac{\partial\Theta}{\partial y}\right]+\frac{\overline{H}}{H-z_g}\left[\frac{\partial}{\partial z^*}(-\overline{w\theta})+\frac{1}{\rho C_p}\frac{\partial R_N}{\partial z^*}\right]. \tag{5}$$

The last two terms are the contributions from divergence of the sensible heat flux and divergence of the radiation field. R_N is the long wave radiation flux.

Equation 6 describes the conservation of moisture mixing ratio.

$$\frac{DQ_v}{Dt}=\frac{\partial}{\partial x}\left[K_x\frac{\partial Q_v}{\partial x}\right]+\frac{\partial}{\partial y}\left[K_y\frac{\partial Q_v}{\partial y}\right]+\frac{\overline{H}}{H-z_g}\frac{\partial}{\partial z^*}(-\overline{wq_v}). \tag{6}$$

An important difference between the higher order turbulence models such as this one and simpler models is the treatment of turbulent fluxes, described by equations 7 and 8[5].

$$\overline{uw}=-1qS_M\frac{\partial U}{\partial z}. \tag{7}$$

$$\overline{w\theta}=-\alpha lqS_M\frac{\partial\Theta}{\partial z}. \tag{8}$$

The turbulent fluxes involve two other factors: l, and q in addition to the gradients and the factor $\tilde{S}_M$ which is a function of the flux Richardson number. Simpler models would use some form of the latter two factors, but not q the turbulence speed or l which is the turbulence length scale. q and l are obtained by solving Equations 9 and 10.

$$\frac{D}{Dt}\left(\frac{q^2}{2}\right) = \frac{\partial}{\partial x}\left[K_x\frac{\partial}{\partial x}\left(\frac{q^2}{2}\right)\right] + \frac{\partial}{\partial y}\left[K_y\frac{\partial}{\partial y}\left(\frac{q^2}{2}\right)\right] + \left(\frac{\overline{H}}{H-z_g}\right)^2\frac{\partial}{\partial z^*}\left[q\mathrm{l}S_q\frac{\partial}{\partial z^*}\left(\frac{q^2}{2}\right)\right] - \frac{\overline{H}}{H-z_g}\left(\overline{uw}\frac{\partial U}{\partial z^*} + \overline{vw}\frac{\partial V}{\partial z^*}\right) + \beta g\overline{w\theta_v} - \frac{q^3}{B_1\mathrm{l}}. \tag{9}$$

$$\frac{D}{Dt}(q^2\mathrm{l}) = \frac{\partial}{\partial x}\left[K_x\frac{\partial}{\partial x}(q^2\mathrm{l})\right] + \frac{\partial}{\partial y}\left[K_y\frac{\partial}{\partial y}(q^2\mathrm{l})\right] + \left(\frac{\overline{H}}{H-z_g}\right)^2\frac{\partial}{\partial z^*}\left[q\mathrm{l}S_1\frac{\partial}{\partial z^*}(q^2\mathrm{l})\right] + \mathrm{l}F_1\left[\frac{\overline{H}}{H-z_g}\left(-\overline{uw}\frac{\partial U}{\partial z^*} - \overline{vw}\frac{\partial V}{\partial z^*}\right) + \beta g\overline{w\theta_v}\right] - \frac{q^3}{B_1}\left[1 + F_2\left(\frac{\mathrm{l}}{kz}\right)^2\right]. \tag{10}$$

The development of these Equations and form of the factors is described by Yamada[6] and Mellor and Yamada[7].

Within the soil, Equation 11 applies:

$$\frac{\partial T_s}{\partial t} = \frac{\partial}{\partial z_s}\left(K_s\frac{\partial T_s}{\partial z_s}\right). \tag{11}$$

A key feature of the model is its description of the surface energy budget Equation 12.

$$R_s + R_L\downarrow - R_L\uparrow = H_s + LE + G_s. \tag{12}$$

R_s is the solar shortwave radiation flux, while $R_L\downarrow$ is the downward long wave atmospheric flux and $R_L\uparrow$ is the blackbody radiation from the surface. The sensible heat flux H_s, is given by:

$$H_s = -\rho_a c_p u^*\theta^*. \tag{13}$$

where u^* is the friction velocity and θ^* is a temperature scale which is defined by:

$$\theta^* = \frac{k}{P_r} \frac{(\Theta(z_1) - \Theta_G)}{\left[In\left(\frac{z_1+z_{0t}}{z_0}\right) + In\left(\frac{z_0}{z_1}\right) - \Psi\right]}. \tag{14}$$

In Equation 14, Ψ is a stability correction factor which is zero during neutral atmospheric stability. Similar expressions are used to define u^* except that velocity at the ground is zero. LE is the latent energy flux and G_s is the soil heat flux. Equations 15 and 16 describe these variables.

$$LE = \rho_a L u^* Q^*. \tag{15}$$

$$G_s = -K_s \frac{\partial T_s}{\partial z_s}|_G. \tag{16}$$

THE PARTICLE TRANSPORT CODE RAPTAD

Model Formulation

RAPTAD is a Monte Carlo random particle statistical diffusion code, developed by Ted Yamada[8]. Pseudo-particles are transported with instantaneous velocities that include the mean wind field and the turbulence velocities. The turbulence velocity is generated randomly consistent with the standard deviation of the wind at the particle location. The location of each pseudo-particle represents the center of mass of a concentration distribution for each puff. The total concentration at any point is obtained by adding the concentration contributions of each puff at that point (a kernel method).

Other particle transport codes produce concentrations by counting particles within a sampling volume. The computed concentration level could vary considerably depending upon the size of the sampling volume and number of particles used in the computation. For example, if the sampling volume is very small, the concentration distribution becomes excessively variable in space. On the other hand, if the sampling volume is too large, the concentration distribution will be over smoothed. The kernel method avoids this difficulty and provides smooth concentration distributions with relatively few particles.

The first step is to calculate the positions and turbulence history of a group of pseudo-particles that represent the emissions from a release. Locations of particles are computed from:

$$x_i(t + \Delta t) = x_i(t) + U_{pi}\Delta t \tag{17}$$

where

$$U_{pi} = U_i + u_i \tag{18}$$

$$u_i(t + \Delta t) = au_i(t) + b\sigma_{u_i}\zeta + \delta_{i3}(1 - a)t_{Lx_i}\frac{\partial}{\partial x_i}(\sigma_{u_i}{}^2) \tag{19}$$

$$a = \exp\left(-\frac{\Delta t}{t_{Lx_i}}\right) \tag{20}$$

and

$$b = (1 - a^2)^{1/2} \tag{21}$$

In the above expressions U_{pi} is the particle velocity in the x_i direction, U_i is the mean velocity, u_i is the turbulence velocity, ζ is a random number from a Gaussian distribution with zero mean and unit variance, t_{Lxi} is the Lagrangian integral time scale for the velocity u_i, σ_{u_i} is the variance of the velocity fluctuation u_i, and δ_{i3} is the Dirac delta. The last term on the right hand side of Equation 19 was introduced by Legg and Raupach[9] to prevent the accumulation of particles in low-energy areas. The mean velocity U_i and vertical velocity variance σ_i are obtained from the output of HOTMAC.

The Monte Carlo kernel method requires that a functional form for the distribution kernel be chosen and that parameters that describe the width, breadth, and depth of the distribution be calculated. Various functional forms can be assumed to express the concentration distribution in the puff. One of the simplest ways is to assume a Chapeau distribution where variances are determined as the time integration of the velocity variances encountered over the history of the puff. The concentration level at a given time and space is determined as the sum of the concentrations each puff contributes. The concentration χ at (X, Y, Z) is estimated by using the following expression:

$$\chi(X,Y,Z) = \frac{Q\Delta t}{(2\pi)^{3/2}}\sum_{k=1}^{N}\frac{1}{\sigma_{x_k}\sigma_{y_k}\sigma_{z_k}}\left(1 - \frac{abs(X_k - X)}{\sqrt{2\pi}\sigma_{x_k}}\right) \tag{22}$$
$$\bullet\left(1 - \frac{abs(y_k - Y)}{\sqrt{2\pi}\sigma_{y_k}}\right)$$
$$\bullet\left\{\left(1 - \frac{abs(z_k - Z)}{\sqrt{2\pi}\sigma_{z_k}}\right) + \left(1 - \frac{abs(z_k + Z - 2z_g)}{\sqrt{2\pi}\sigma_{z_k}}\right)\right\}$$

where (x_k, y_k, z_k) is the location of the k^{th} particle; σ_{xk}, σ_{yk}, and σ_{zk} are standard deviations and z_g is the ground elevation. The variances are estimated based on Taylor's homogeneous diffusion theory[10]. For example σ_y is obtained from

$$\sigma_y^2 = 2\sigma_v^2 \int_o^t \int_o^\zeta R(\zeta) d\zeta dt \tag{23}$$
$$= 2\sigma_v^2 t_{Ly} \left(t + t_{Ly} \exp\left(-\frac{t}{t_{Ly}}\right) - t_{Ly} \right)$$

where a correlation function $R(\zeta) = \exp\left(\frac{-\zeta}{t_{Ly}}\right)$ is used. Equation 23 is approximated by

$$\sigma_y = \sigma_v t \; t \leq 2t_{Ly} \tag{24}$$

and

$$\sigma_y^2 = 2t_{Ly}\sigma_v^2 t \; t > 2t_{Ly} \tag{25}$$

Although the turbulence field is not normally homogeneous, we assume the theory can be applicable over a short time period, such as an integration time step. Therefore,

$$\sigma_y(t + \Delta t) = \sigma_y(t) + \sigma_v \Delta t \; t \leq 2t_{Ly} \tag{26}$$

and

$$\sigma_y^2(t + \Delta t) = \sigma_y^2(t) + 2t_{Ly}\sigma_v^2 \Delta t \; t > 2t_{Ly} \tag{27}$$

are used. Similar relations are used for the x and z directions. The standard deviations σ_u, σ_v, and σ_w at each particle location are obtained by interpolating grid values of a computation grid volume in which a particle is located.

RAPTAD served as the jumping off point for a new model called RAPBOX. RAPBOX uses the RAPTAD formulation to describe the positions of pseudo-particles and associated sigmas. The domain encompassed by the psuedo-particle positions is divided into cells. In the applications reported herein there are 9 x 9 x 9 cells. The x -axis of the cell coordinate system is oriented in the initial direction of travel (with the wind at the source), with the y-axis normal to the x-axis, and the z-axis is vertical. The domain of the cells extends from the minimum x particle position minus three times the maximum σ_x to the maxium x

particle position plus three times the maximum σ_x, with similar extensions in the y-direction. In the vertical the cells extend from z_u, the maximum elevation of the particles plus three times the maximum σ_z to z_l which is the ground unless the ground elevation is lower than the larger of z_{pl} and $z_m - H_{eff}$. z_{pl} is the lowest particle position minus three times the maximum σ_z. While $z_m - H_{eff}$ is the mean height minus the effective stack height. Letting the coordinate system extend to the mean height minus the effective stack height reduces the vertical definition of the plume but it avoids the dramatic changes in the cell volume and location which would otherwise occur during fumigation of an elevated plume.

The side walls of the cells are oriented along the transformed x and y axes, but the tops and bottoms of the cells are not necessarily horizontal planes because of the terrain irregularities. The bottom surface of the bottom cell is defined by two intersecting planes. One plane includes the points (x_i, y_j, z_{lij}), $(x_{i+1}, y_j, z_{li+1j})$, and $(x_{i+1}, y_{j+1}, z_{li+1j+1})$ while the other includes the points (x_i, y_j, z_{lij}), $(x_i, y_{j+1}, z_{lij+1})$, and $(x_{i+1}, y_{j+1}, z_{li+1j+1})$. The cells equally divide the vertical domain. Figure 1 depicts a cell.

RAPBOX initially computes the particle positions over the first hour of travel before the photochemistry cells are defined. RAPBOX then computes the concentrations of NOX at each of the cell centers and the corresponding mean winds and the σs. It also computes temperatures and the volume correction to standard conditions. At the next cell computation interval, normally five minutes later, the model computes the fraction of the cell volume which has been advected from the same or adjacent cells during the computation interval. It also computes how much NOX concentration has been added to the cell center by pseudo-particles released during the interval. In addition it computes how much cell volume has been exchanged with adjacent cells by turbulent exchange during the interval.

Turbulent volume exchange is calculated by considering the probability that a particle from a cell will escape the cell during the interval. We begin by calculating the σs of particles starting at the center of the cell at the start of the interval. The treatment follows that of Equations 23 through 27 with the initial σ being zero. With the Chapeau function formulation the contribution of particles with a initial position of x' at the point x is:

$$\chi_x = 1 - \frac{abs(x - x')}{\sqrt{2\pi} \cdot \sigma_x} \tag{28}$$

considering only the one-dimensional formulation for simplicity. We assume that within the cell the concentrations are uniform, consequently we can integrate over the all the positions in the cell which are within $\sqrt{2\pi}\sigma_x$ of the boundary at x_1. The fraction of the cell volume

which passes through the boundary x_1 is:

$$F_{d1} = \frac{1}{6}\frac{\sqrt{2\pi}\cdot\sigma_x}{x_2 - x_1}, \tag{29}$$

with similar relations for the y and z directions.

The output of RAPBOX includes: (1) the positions of the cell centers, (2) the NOX concentrations at the cell centers (first output set only; others are zero), (3) the NOX concentrations at the cell centers associated with NOX emissions during the time interval, (4) the fraction of the cell volume which has been advected into the cell from the cell or adjacent cells during the preceding interval, and (5) the fraction of the cell volume which has been exchanged with adjacent cells during the interval. The file is a large file since for each cell at each time interval there are 27 cells involved with advection and 4 modes of dispersion. Because cell center parameters are used volumes exchanged in the forward (+x) and backward (-x) directions are the same and similarly for the left and right directions.

THE PHOTOCHEMISTRY CODE

The photochemistry code is based on the carbon bond IV system [3] with additional reactions which describe the formation of sulfates and the formation of new particles and changes in the particle size distribution. The sulfate formation scheme is based on the reactions:

$$SO_2 + OH \rightarrow SO_4 + HO_2,$$

$$XO_2 + SO_2 \rightarrow SO_4,$$

$$O + SO_2 \rightarrow SO_4.$$

The additional reactions relating to particle formation and size distribution changes are:

$$HNO_3 + NH_3 \rightarrow NH_4SO_4,$$

$$2cn \rightarrow cn,$$

$$NH_4NO_3 \rightarrow \gamma cn + NH_4NO_3,$$

$$SO_4 \rightarrow \beta cn + SO_4,$$

$$2ca \rightarrow ca,$$

$$ca + cn \rightarrow \alpha va + ca,$$

$$SO_4 \rightarrow \alpha_1 va,$$

$$NH_4NO_3 \rightarrow \alpha_2 va,$$

$$NH_4NO_3 \rightarrow NH_3 + HNO_3.$$

The particle formation reactions are based on a system in which the size distribution is composed of an accumulation mode and a condensation mode. Both modes are lognormal. There are three variables to be solved for in this system: (1) the number concentration in the condensation mode cn, (2) the number concentration in the accumulation mode ca, and (3) the accumulation volume concentration va. In this model the mean geometric diameter of the condensation mode, dg_{nn}, the standard deviation of the condensation mode, sg_n and the standard deviation of the accumulation mode size distribution, sg_a are input. The geometric mean diameter of the number distribution of the accumulation mode, dg_{na}, is given by:

$$dg_{na} = 4.209e^{-.9753sg_a} \cdot \left(\frac{va}{ca}\right)^{\frac{1}{3}}. \tag{30}$$

The carbon bond system is a widely used system for atmospheric photochemical models. The carbon bond IV formulation is appropriate for dealing with the effects of methane, isoprene, and other hydrocarbons found in a relatively clean rural environment.

The model calculates the sun angle and uses photochemical decay constants based on elevation of 6000 feet for either summer or winter conditions. The appropriate rates were developed based on radiative transfer calculations and will differ somewhat from the sea level values normally used in other photochemical models.

The model uses a stiff equation solver to compute the changes produced by chemical reactions, transport, and diffusion. The additional terms associated with advection take the form:

$$\Delta C_{ijk} = \sum_{lmn \neq ijk} Fr_{lmn \rightarrow ijk} Clmn - (1 - Fr_{ijk \rightarrow ijk}), \tag{31}$$

while the terms associated with diffusion are:

$$\Delta C_{ijk} = \tag{32}$$

$$P_{i+1,jk \rightarrow ijk} C_{i+1,jk} + P_{i-1,jk \rightarrow ijk} C_{i-1,jk} + \tag{33}$$

$$P_{ij+1,k\rightarrow ijk}C_{ij+1,k} + P_{ij-1,k\rightarrow ijk}C_{ij-1,k} + P_{ijk+1\rightarrow ijk}C_{ijk+1} + P_{ijk-1\rightarrow ijk}C_{ijk-1} - C_{ijk}\sum_{ijk\neq lmn} P_{ijk\rightarrow lmn}.$$

When the concentrations indices are beyond their defined ranges the background concentration is used instead. Background concentrations are calculated from initial conditions using the stiff equation solver, so that the background calculations reflect the changes expected with sun angle.

COMPARISONS OF MODEL PREDICTIONS WITH OBSERVATIONS

The Experimental Dataset

Four separate southwestern experimental datasets were chosen for comparison. All sets involve airplane tracings of the plume from the Navajo Generating Station, a large coal-fired power plant located in northern Arizona. Each of the sets includes measurements of ozone, NO_2, NO, sulfates, and nitrates. Two of the sets come from the VISSTA experiments[11] and represent plume trackings during a winter day (December 13, 1979) and a summer day (July 13, 1979). Plumes were traced to a downwind distance of 89 km in the summer and 115 km in the winter. The published data for the July 13 case represent a relatively complete set of emissions and meteorology while there were less details published on the winter experiment.

The other two sets represent measurements[2] made in August of 1980 were notable. One, on the afternoon of the 27^{th}, included a tracing of 140 km during steady winds and there were indications of ozone formation in the plume. The other was in the predawn morning of the same day and involved an interaction with plume height terrain during stable conditions. Unfortunately, at the time of the preparation of this paper the reports describing the details of the study were not available. The published data did include a number of details which allow some of the missing details to be filled in. For instance the morning flight provides the location of the terrain so that approximate wind directions can be deduced. The afternoon flight reports the travel time so that wind speeds can be deduced.

Approximate meteorological conditions for the August flights were derived from the 850, 700, and 500 mb charts for the same time. The charts suggest that the early morning winds were from approximately that southwest to west-southwest at about 5-6 m/s. Later in the day the winds would have been more westerly with speeds of about 4 m/s. Unfortunately, emissions were not reported for either flight.

Model Input

The photochemical model requires an initial plume distribution with levels of all species defined for a specific NOX concentration. For species such as NOX, SO2, and aerosol volume, the initial concentration in a cell is proportional to the calculated NOX for the cell. For species such as ozone which are depleted in a rich NO environment, there are two situations. If the ratio, rat, of the calculated NOX to the initial plume NOX is greater than 1, the initial plume values are used. If rat is less than one, the cell concentration, yc, is calculated as:

$$yc = rat \cdot ys + (1 - rat) \cdot yb, \tag{34}$$

where ys is the initial plume concentration of the depleted species and yb is its background concentration.

The background concentrations for reactive hydrocarbons play a major role in the photochemistry. For this work background levels for light hydrocarbons were taken as the median values measured in the Lake Powell Research Project[12] in remote areas near the Navajo Generating Station. Values for isoprene were based on calculated values developed by investigators[13] in Colorado. Their calculations were consistent with their measurements in a remote region of Colorado. It is important to remember that their values and the other hydrocarbon values were taken as representative of midday conditions. Thus these values would not necessarily serve as appropriate initial conditions. Typically, isoprene and olefins were rapidly depleted in the background atmosphere during the course of the model run. Consequently somewhat higher initial concentrations were required to obtain noon time values consistent with daytime background values.

Results

The dawn flight on August 27, 1980 represents an interesting case where high terrain influenced plume behavior. Figure 2 reports the modeled wind fields at initial plume height above ground. Figure 3 reports the predicted wind field near the surface. The investigators[2] reported that the terrain permitted mixing into the plume. Figure 4 shows the plume cross section after the first half hour of travel. Note that the boundaries are taken as background so that cell 2 is the first model calculated value and that the concentrations have been scaled by 10000. At about 65 km the plume has interacted with the high terrain and produced considerable mixing as shown in Figure 5. The model domain is about 3.2 km by 900 meters deep, whereas at 17 km the plume was about 2.5 km in width and 750 meters deep. However, the measurements suggest a more dilute plume with NOX concentrations of .010ppm versus .029ppm for the model. The predicted SO2 to sulfate conversions was about .07% at the plume center rising to .3% away from the center while the measured value was .95%. The nitrate conversions were about .03% which is very low compared to the measured value of 11%.

The afternoon of the 27^{th} represents another interesting case. This was the plume which was tracked to the greatest distance and some indication of ozone formation was found. Figure 6 reports the ozone concentration pattern about 2 hours downwind, while Figure 7 reports the pattern at 7 hours downwind. For comparison Figure 8 reports the ozone concentration pattern at 8.5 hours downwind. We can see that the ozone was initially depleted throughout the plume, but that an off plume bulge formed at 7 hours and spread at 8.5hours. Figure 9 reports the concentration pattern for a stable tracer with emissions equivalent to the total NOX. By comparison with Figure 8 we can see that the highest ozone concentrations do not occur in the center of the plume. Both Sulfate and Nitrate formation were very small compared to the measurements.

The ozone formation appears to be associated with very dilute portions of the plume mixing into background air with very little NOX. Trainer et al [13] reported that small amounts .2 to 2 ppb could produce ozone when combined with methane and isoprene.

The July 13 case gave ozone depletions throughout the plume travel. The deficits were approximately comparable to the measured ones. The predicted sulfate sulfur at 2.5 hours downwind was about .16% while the measurements reported .08%. At 4.5 hours downwind the predicted value was .3% versus a measured value of 1.6%. Once again the nitrates were

relatively small.

The July 13 case displayed a simulation of inversion breakup. Figure 10 displays a well defined plume aloft after 1.5 hours of travel. Figure 11 shows the concentration patterns after breakup and mixing at 3.25 hours downwind

The December 13 case gave ozone depletion throughout the plume travel. Once again the nitrates were very low. Sulfate concentrations were less than .01%, but the measurements also showed very low values.

CONCLUSIONS

A model has been developed which shows promise for addressing the photochemistry of plumes. The model is driven by a three dimensional prognostic atmospheric circulation code. It simulates stagnation, inversion breakup, and high terrain interactions. It is used to provide input for a moving cell dispersion and diffusion model. Finally a photochemical model solves the chemical balance equations for each cell. The model can provide definition of plume structure which would be very hard to obtain with Eulerian codes.

Comparison of the model results to experiments shows ozone formation similar to measurements, however nitrate formation is greatly underestimated. Sulfate formation is closer to measured values, but is generally underestimated. It is clear that further attention to the nitrate and sulfate chemistry is required.

ACKNOWLEDGMENTS

The work is supported by the Los Alamos National Laboratory and was performed under the auspices of the US Department of Energy at Los Alamos National Laboratory.

REFERENCES

1. D. D. Davis, G. Smith, and G. Klauber, "Trace Gas Analysis of Power Plant Plumes Via Aircraft Measurement: O3, NOx, and SO2 Chemistry," Science, vol. 186, pp 733-735 (1974).

2. L. W. Richards, J. A. Anderson, D. L. Blumenthal, J. A. McDonald, P. S. Bhardwaja, R. B. Candelaria, and D. W. Moon, "Nitrogen and Sulfur Chemistry and Aerosol Formation in a Western Coal-Fired Power Plant Plume," in Transactions - Visibility and Fine Particles, TR-17, Air and Waste Management Association, pp 242-259 (1990).

3. Michael W. Gery, Gary Z. Whitten, James P. Killus, and Marcia C. Dodge, "A Photochemical Kinetics Mechanism for Urban and Regional Scale Computer Modeling," Journal of Geophysical Research, vol. 94, no. d10, pp. 12925-12956 (1989).

4. T. Yamada, "Numerical Simulation of the Night 2 Data of the 1980 ASCOT Experiments in the California Geysers Area," Archives for Meteorology, Geophysics, and Bioclimatology, Ser. A34, pp 223-247 (1985).

5. T. Yamada, "The Critical Richardson Number and the Ratio of the Eddy Transport Coefficients Obtained from a Turbulence Closure Model," J. Atmos. Sci., vol 32 pp926-933 (1975).

6. T. Yamada, "A Numerical Simulation of Nocturnal Drainage Flow," J. Meteor. Soc., Japan, vol 59, pp 108-122 (1981).

7. G. I. Mellor, and T. Yamada, "Development of a Turbulence Closure Model for Geophysical Fluid Problems," Rev. Geophys. Space Phys., vol 20, pp 851 875 (1982).

8. T. Yamada, and S. Bunker, "A Numerical Model Study of Nocturnal Drainage Flows with Strong Wind and Temperature Gradients," it J. Appl. Meteor., (submitted, 1988).

9. R. J. Legg and M. F. Raupach, "Markov-Chain Simulation of Particle Dispersion in Inhomogeneous Flows: The Mean Drift Velocity Induced by a Gradient in Eulerian Velocity Variance," Boundary-Layer Meteorol., vol 24 pp3-13 (1982).

10. G. I. Taylor, "Diffusion by Continuous Movements," Proceedings of the London Mathematical Society, Ser. **2**, vol 20 pp196-211 (1921).

11. L. W. Richards, J. A. Anderson, D. L. Blumenthal, A. A. Brandt, J. A. McDonald, N. Waters, E. S. Macias, and P. S. Bhardwaja, "The Chemistry, Aerosol Physics, and Optical Properties of A Western Coal-Fired Power Plant Plume," Atmospheric Environment, vol. 15, pp 2111- 2134 (1981).

12. E. G. Walther, W. C. Malm, and R. Cudney, "The Excellent But Deteriorating Air Quality in the Lake Powell Region," Lake Powell Research Project Bulletin number 52, National Science Foundation, Research Applied to National Needs (1978).

13. M. Trainer, E. Y. Hsie, S. A. McKeen, R. Tallamraju, D. D. Parrish, F. C. Fehsenfeld, and S. C. Liu, "Impact of Natural Hydrocarbons on Hydroxyl and Peroxy Radicals at a Remote Site," Journal of Geophysical Research, vol. 92, no. d10, pp 11879-11894 (1987).

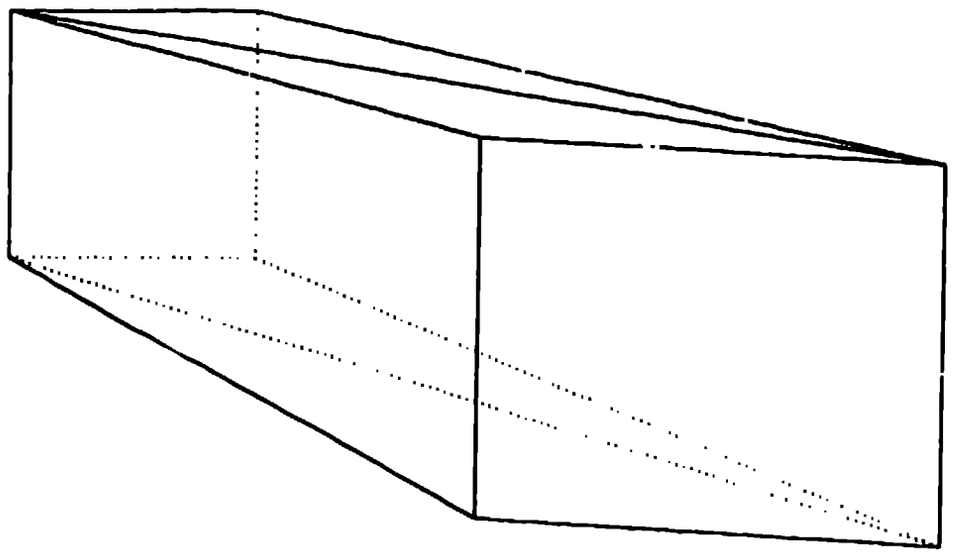

Figure 1: Depiction of a RAPBOX cell.

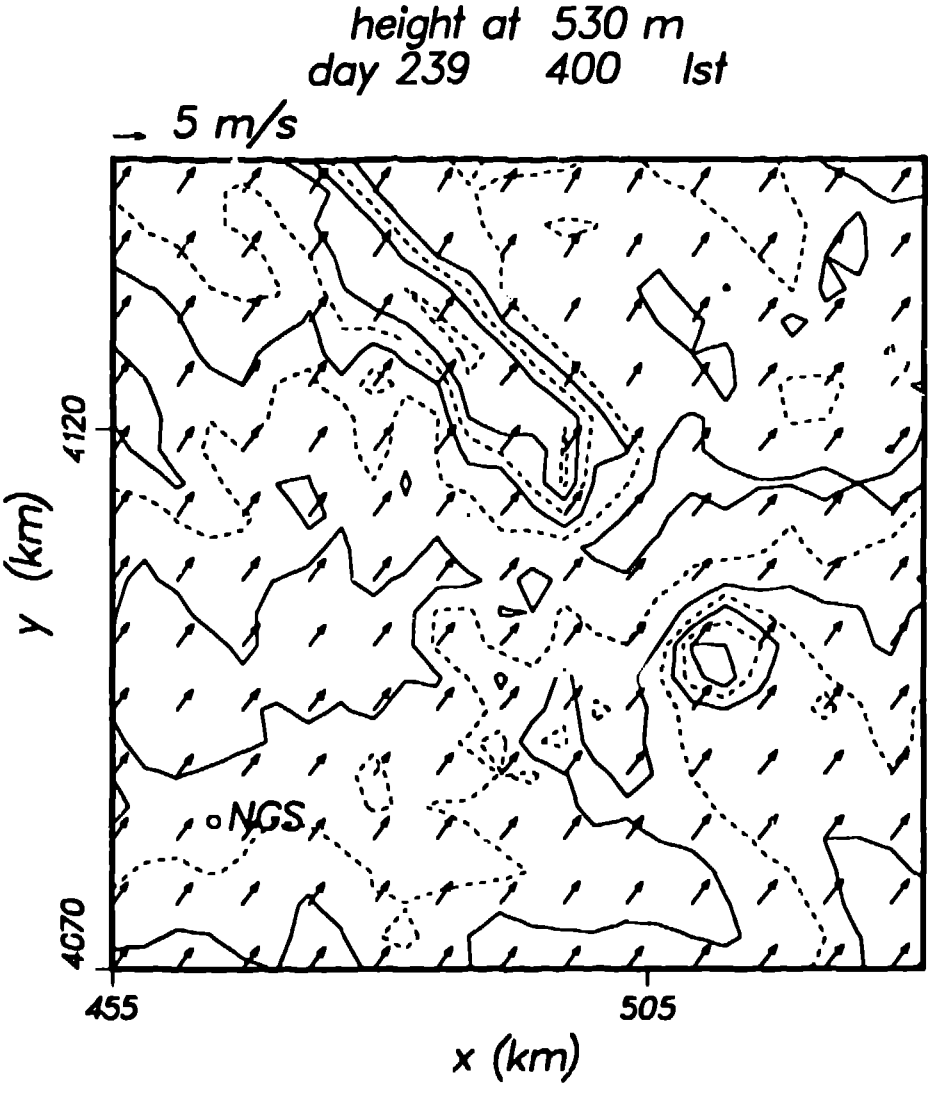

Figure 2: Predicted wind fields during predawn hours of August 27 at initial plume height. Contours are in meters.

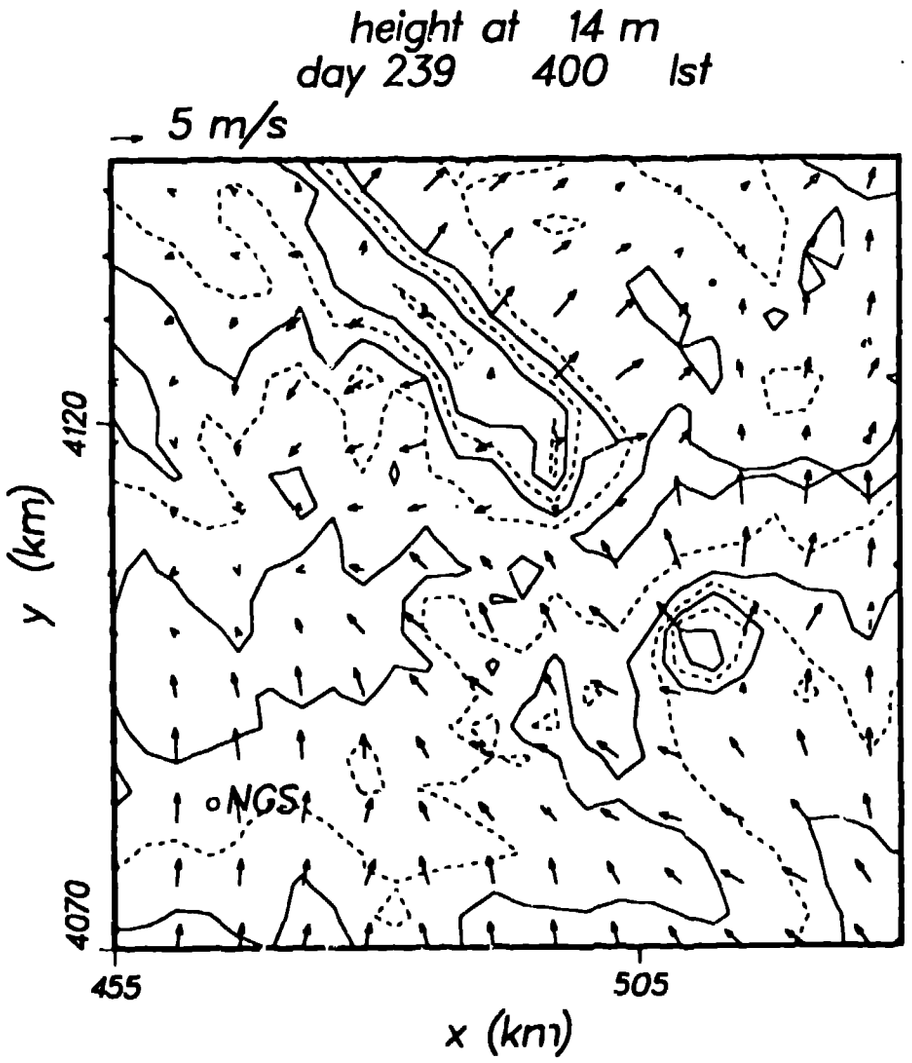

Figure 3: Predicted wind fields during predawn hours of August 27 near the surface. Contours are in meters.

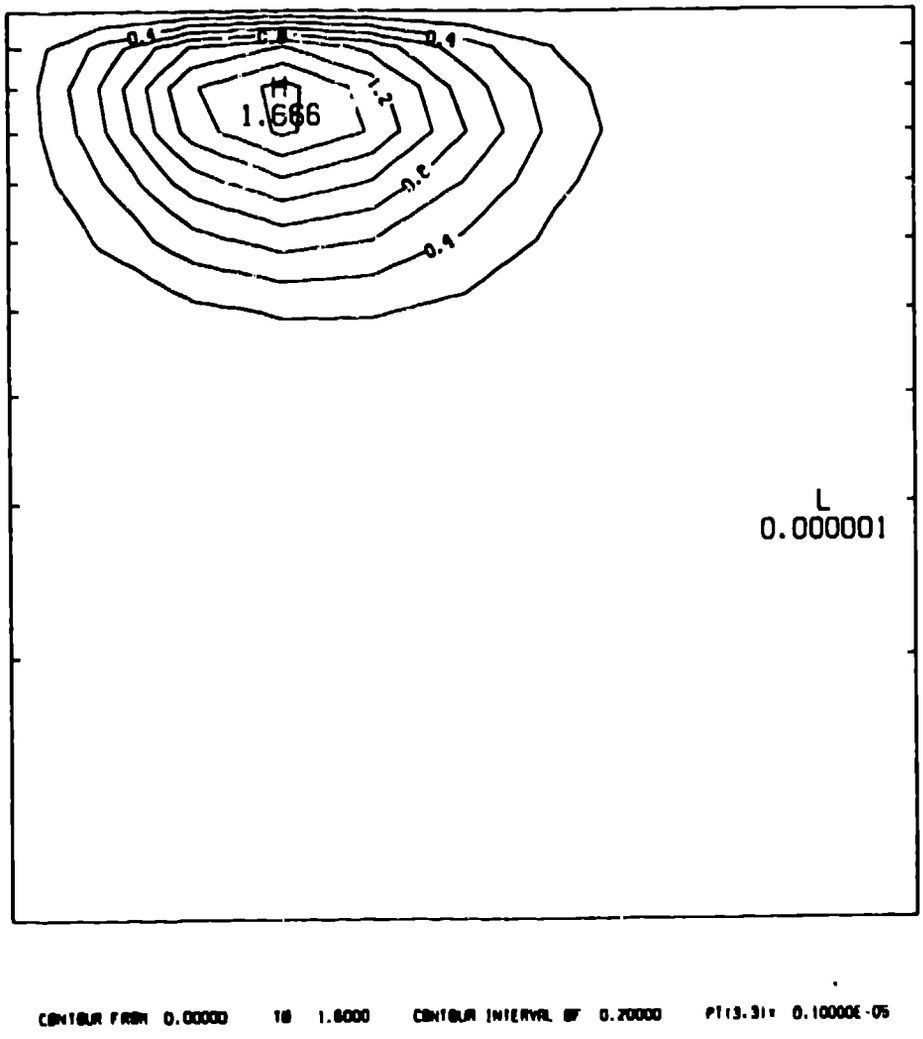

Figure 4: Predicted NOx crosswind concentrations at 11 km downwind before dawn on August 27, 1980.

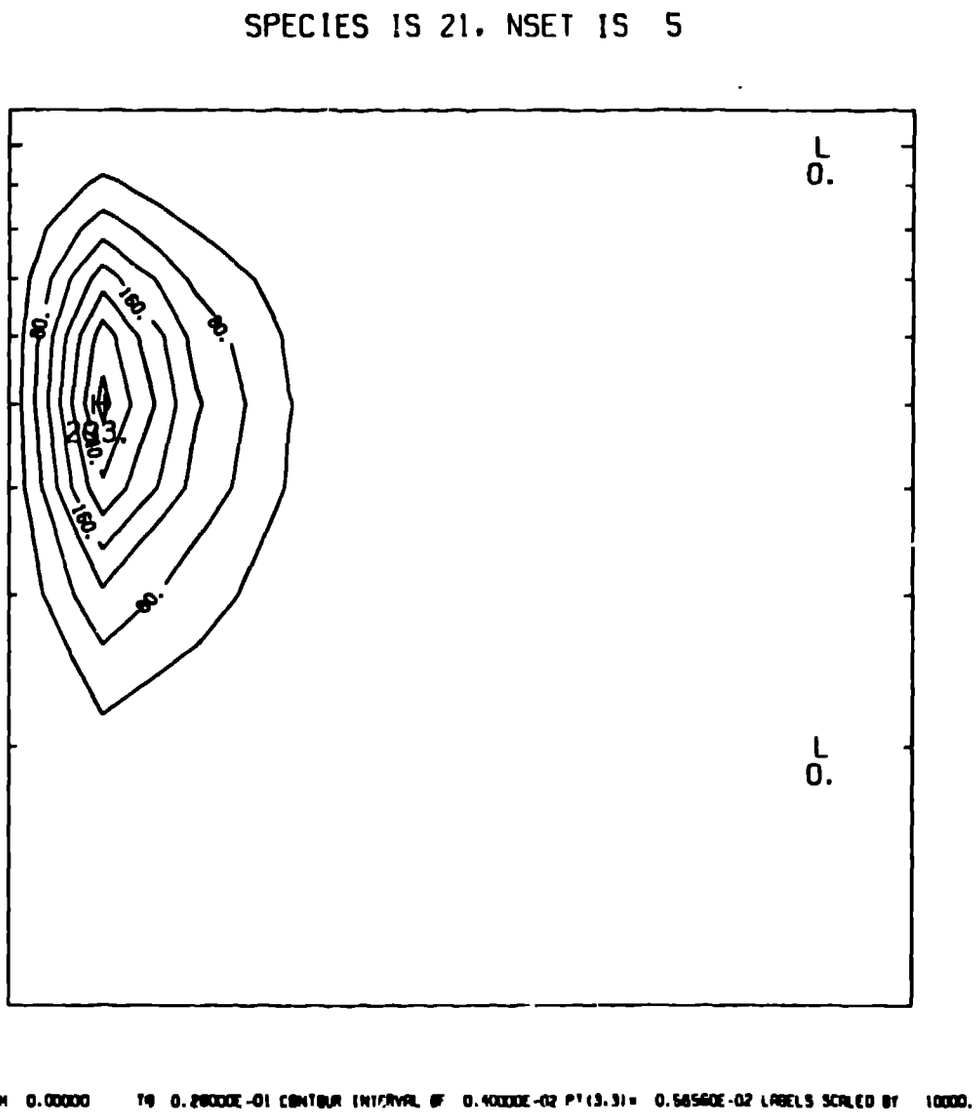

Figure 5: Predicted NOx crosswind concentrations at 65 km downwind before dawn on August 27, 1980.

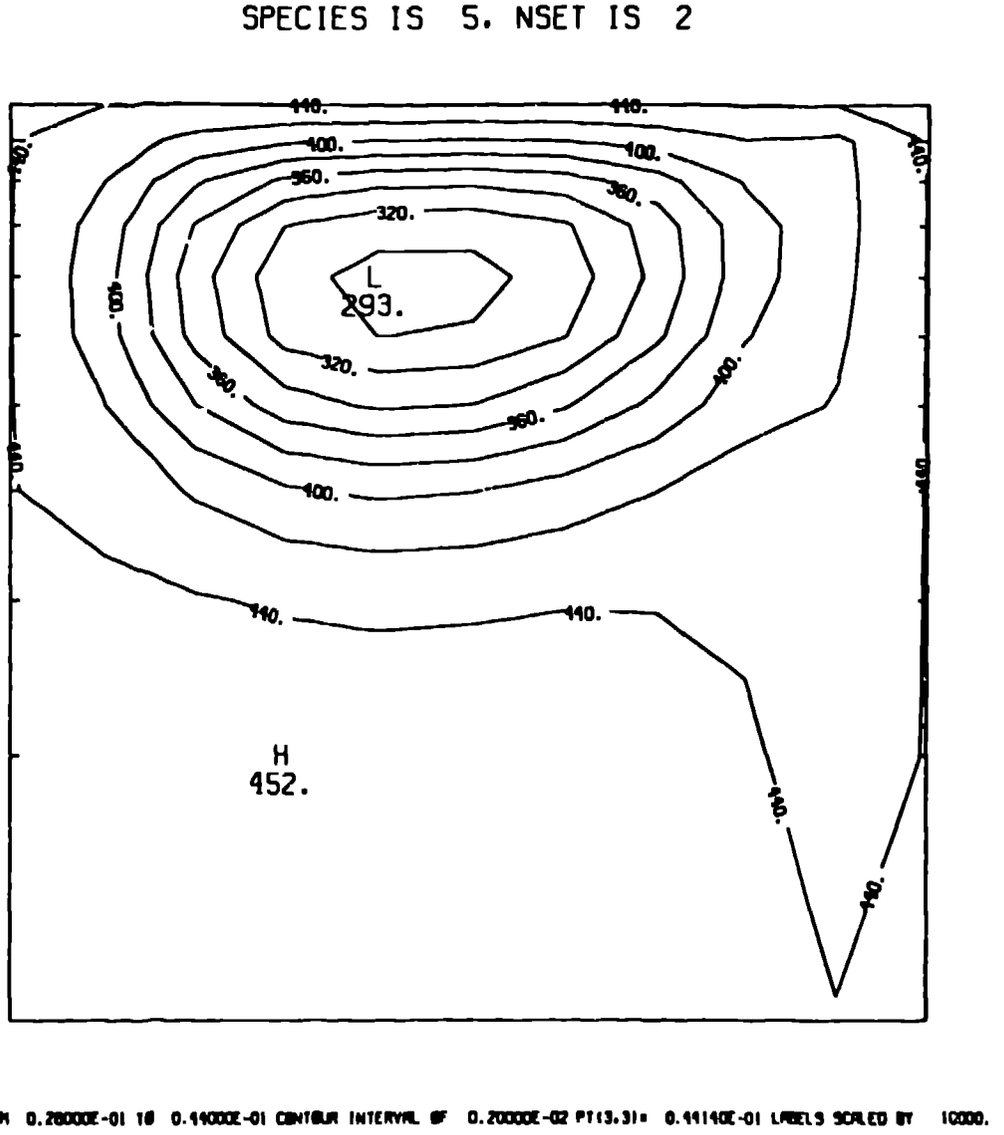

Figure 6: Predicted Ozone concentrations at two hours downwind on the afternoon of August 27, 1980

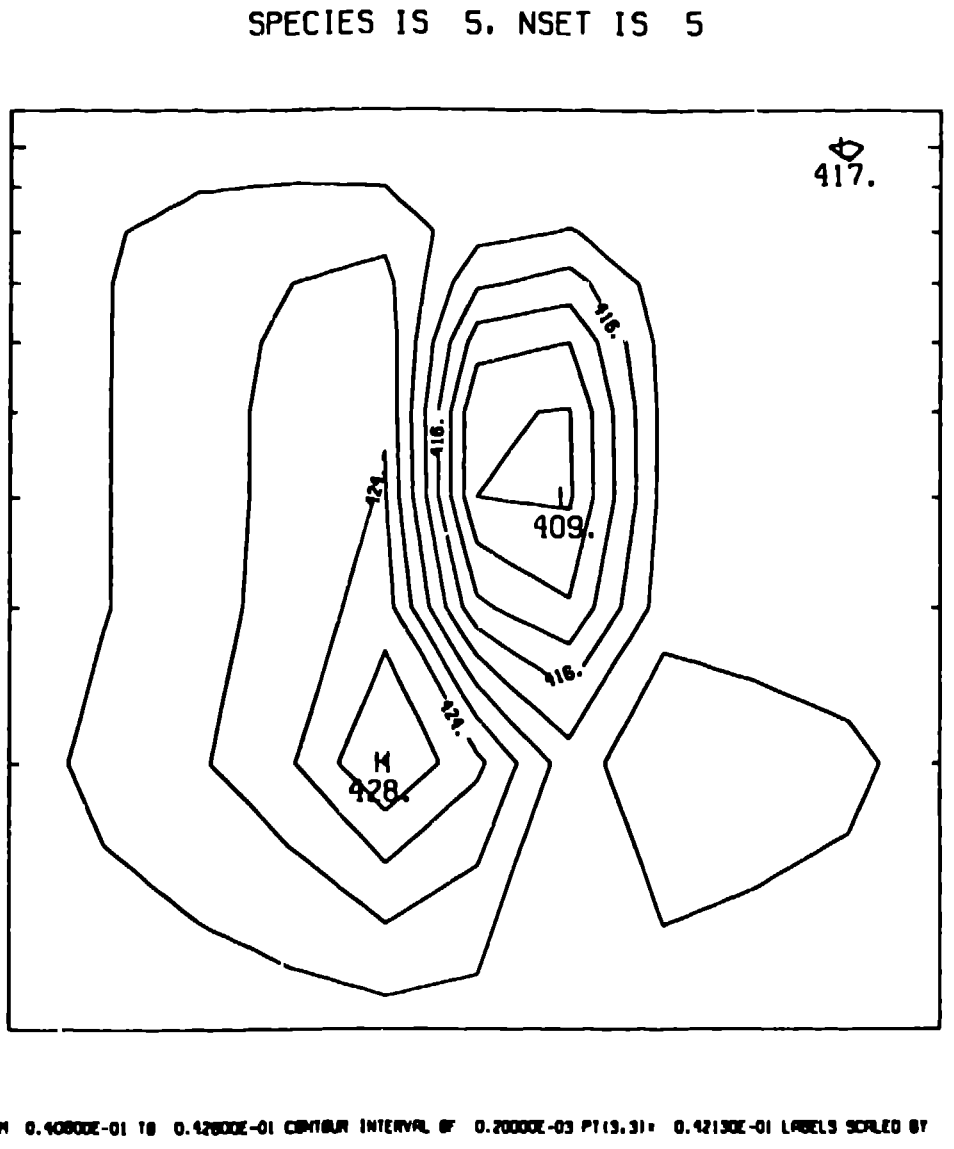

Figure 7: Predicted Ozone concentrations at 7 hours downwind on the afternoon of August 27, 1980

SPECIES IS 5, NSET IS 7

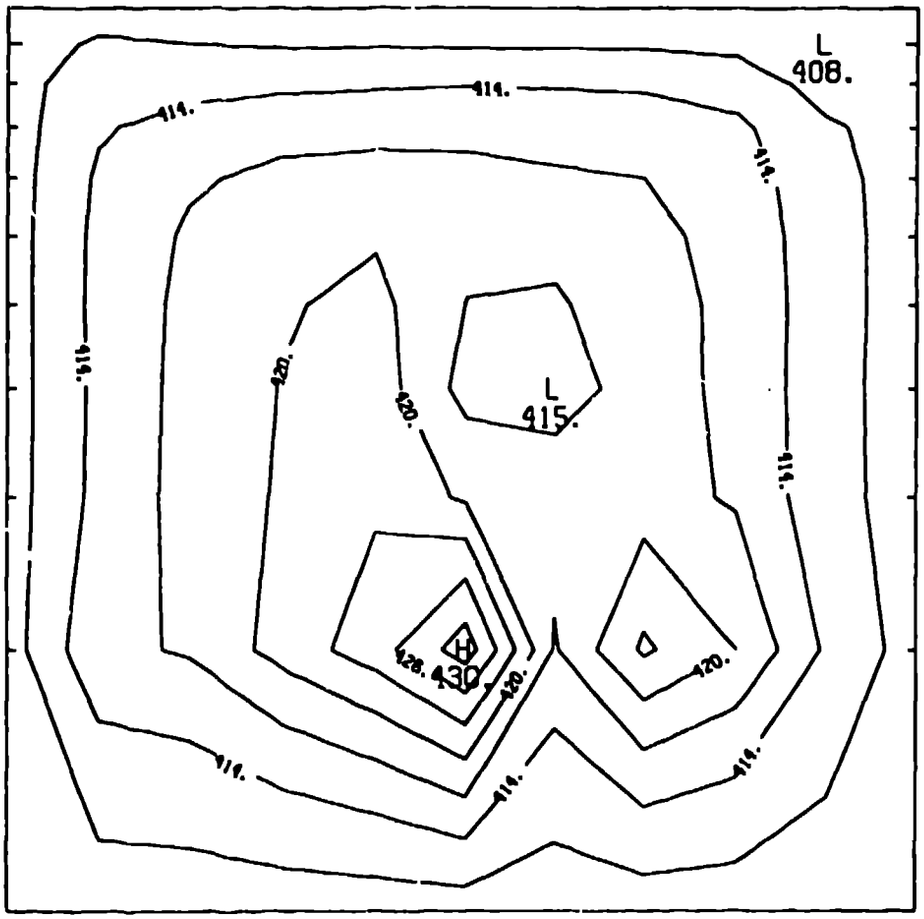

CONTOUR FROM 0.400000E-01 TO 0.429000E-01 CONTOUR INTERVAL OF 0.300000E-03 PTS(5,3)= 0.418100E-01 LABELS SCALED BY 10000.

Figure 8: Predicted Ozone concentrations at 8.5 hours downwind on the afternoon of August 27, 1980

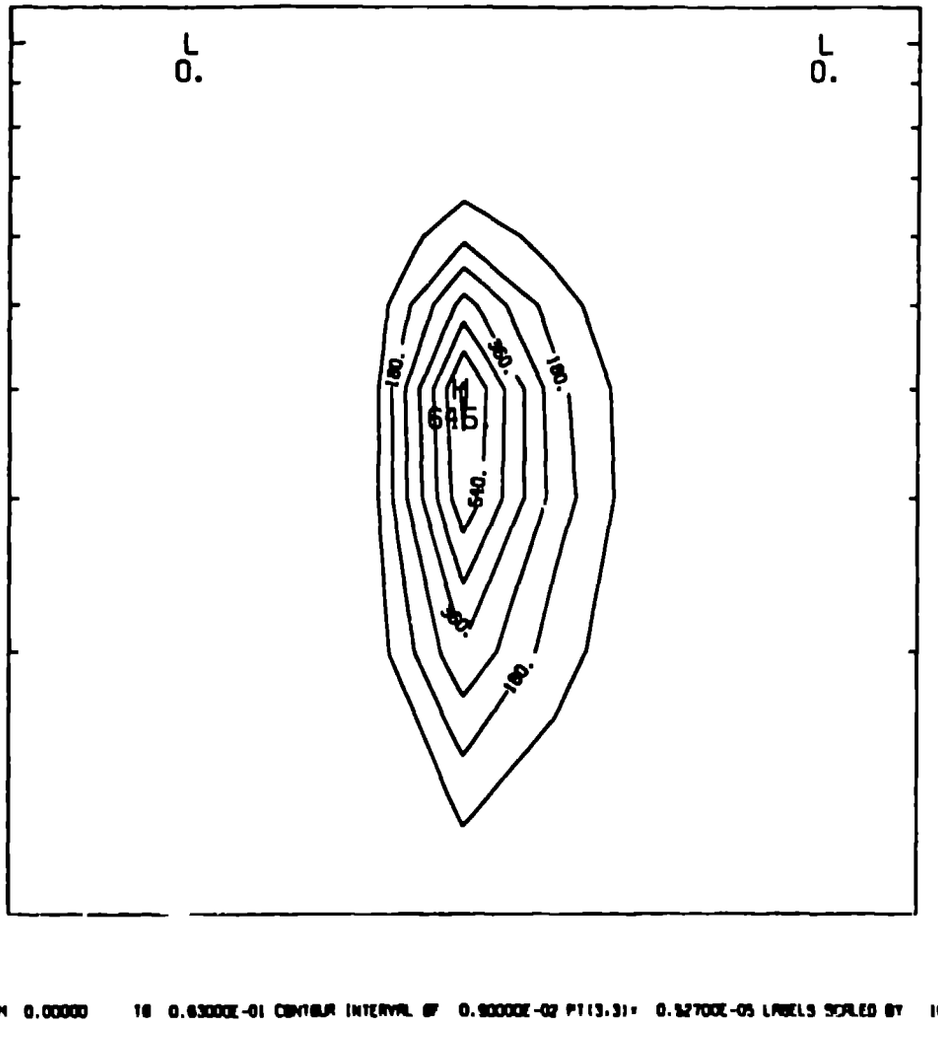

Figure 9: Predicted stable species concentrations at 8.5 hours downwind on the afternoon of August 27, 1980. Emissions are set equal to total NOX emissions

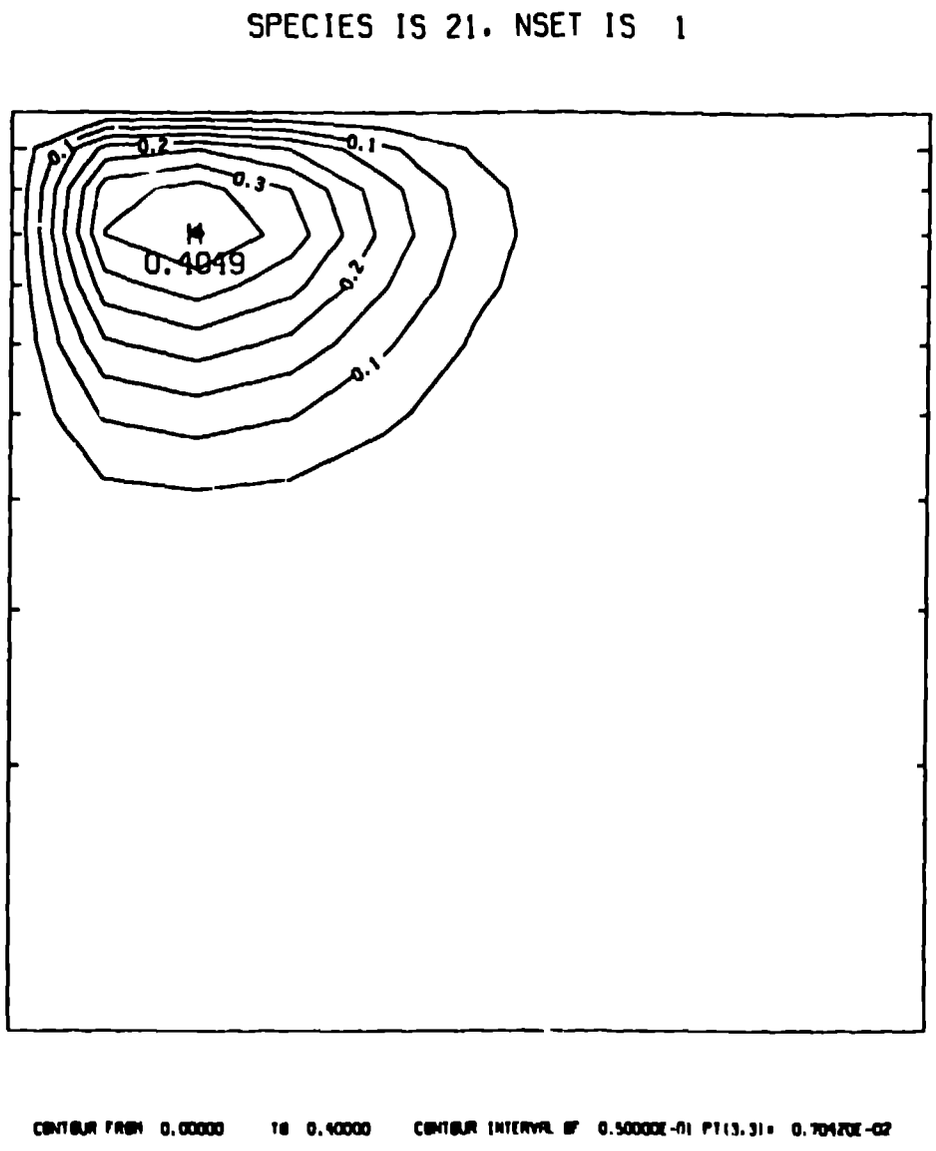

Figure 10: Predicted stable species concentrations at 1.5 hours downwind on July 13,1979. Emissions are set equal to total NOX emissions

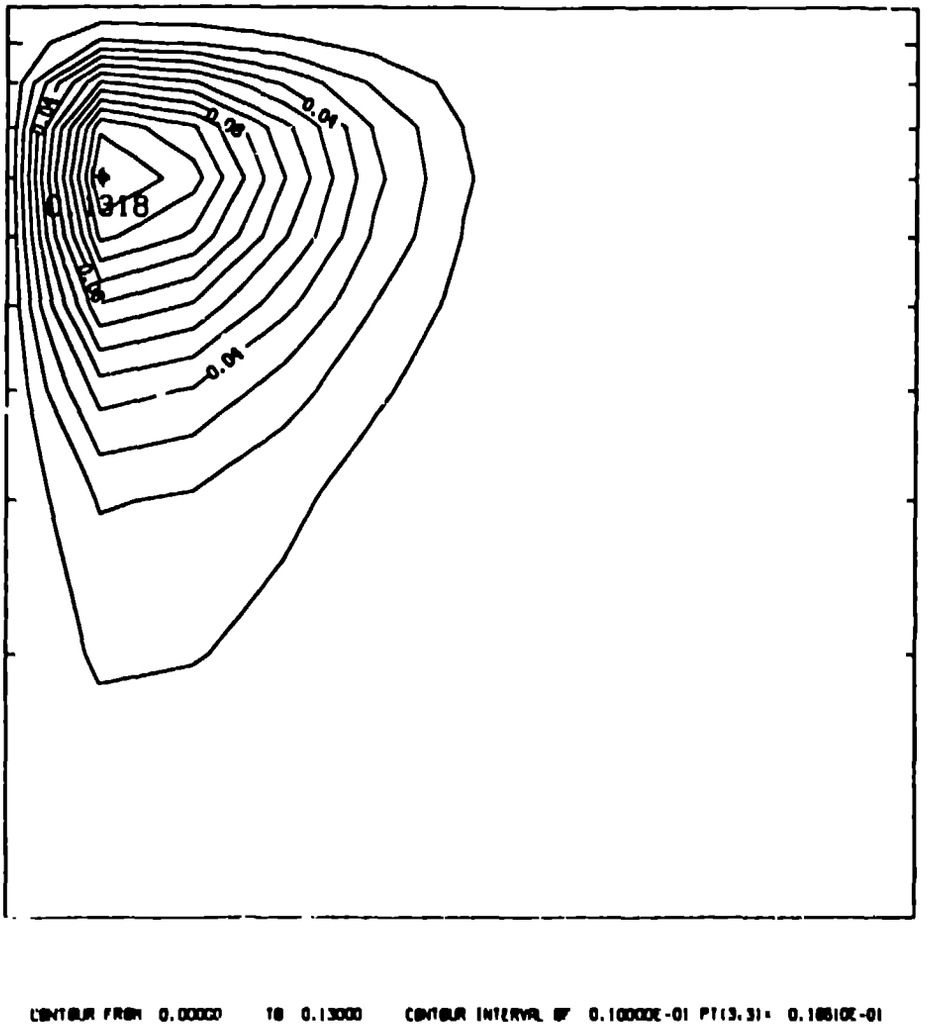

Figure 11: Predicted stable species concentrations at 3 hours downwind on July 13,1979. Emissions are set equal to total NOX emissions